Analytical Theory of Graphene Nanoribbon Transistors

Pei Zhao[†] Mihir Choudhury[‡] Kartik Mohanram[‡] Jing Guo[†]
[†]Department of Electrical and Computer Engineering, University of Florida, Gainesville
[‡]Department of Electrical and Computer Engineering, Rice University, Houston
{peizhao7,guoj}@ufl.edu {mihir,kmram}@rice.edu

Abstract

Graphene has emerged as one of the most promising materials to address scaling challenges in the post silicon era. A simple model for graphene nanoribbon field-effect transistors (GNRFETs) is developed for treating the effects of edge bond relaxation, the third nearest neighbor interaction, and edge scattering, all of which are pronounced in GNRFETs, but not in carbon nanotube FETs.

Index terms: Graphene nanoribbons, analytical model, edge bond relaxation, third nearest neighbor interaction, edge scattering.

1. Introduction

Graphene, which is a monolayer of carbon atoms packed into a two-dimensional honeycomb lattice, has been experimentally demonstrated to possess remarkable carrier transport properties [1–3]. The high mobility and carrier velocity of graphene promises ballistic devices and high switching speeds. Graphene also offers ultra-thin body for optimum electrostatic scaling and excellent thermal conductivity. The potential to produce wafer-scale graphene films with full planar processing for devices promises high integration potential with conventional CMOS fabrication processes, which is a significant advantage over carbon nanotubes.

Two-dimensional graphene is a semi-metal without a band-gap. A band-gap can be obtained by using a narrow graphene nanoribbon (GNR). Unlike carbon nanotubes (CNTs), which are mixtures of metallic and semiconducting materials, a recent experiment [4] demonstrated that all sub-10nm GNRs are semiconducting due to the edge effect, which make them more attractive for electronic device applications.

In this paper, a simple analytical theory of GNR field-effect transistors (GNRFETs) is developed, with an emphasis on examining the edge effects and the C-C interaction across hexagons. The edge bond relaxation and the third nearest neighbor interaction, which are not pronounced in CNTFETs, are found to play an important role in the electronic structure of GNRs and device characteristics of GNRFETs. The effect of edge scattering in GNRFETs, which is caused by non-ideal GNR edges, is also included in our model.

2. Analytical model

A bottom-up, semi-analytical nanotransistor model has previously been applied to model silicon nanoscale MOSFETs, nanowire FETs, and CNTFETs [5–9]. In this work, a GNRFET is modeled by extending the model to treat the effects of edge bond relaxation, the third nearest neighbor interaction, and edge scattering, all of which are pronounced in GNRFETs, but not in CNTFETs.

This research was supported in part by grant N000140810861 from the Office of Naval Research, in part by the Semiconductor Research Corporation, and in part by grant CCF-0701547 from the National Science Foundation.
.

An accurate calculation of the band structure is a necessary input of the model. For CNTs, a simple p_z orbital tight binding (TB) calculation with the first nearest neighbor interaction yields an accurate *E-k* relation in the energy range relevant for carrier transport. In a GNR, this calculation, however, fails to yield even a correct band-gap, as indicated by comparing the TB results to the *ab initio* simulation results [10–12]. In an armchair edge GNR (AGNR), the difference is due to both the edge bond relaxation and the third nearest neighbor interaction (shown in figure 1), which a simple TB calculation does not include. The second nearest neighbor, which only shifts the dispersion relation in energy direction, does not change the band-gap and is not included in our model. A re-parameterization of the TB model by introducing additional parameters describing these effects, however, can yield band-structure in agreement with the *ab initio* calculations in the energy range of interest [12]. The E-k dispersion can be expressed as

$$E = \pm\sqrt{(\Delta/2)^2 + (\hbar v_{\rm s} k)^2} \tag{1}$$

where

$$\Delta/2 = \gamma_1\left(1 + 2s\cos\frac{p\pi}{m+1}\right) + \gamma_3\left(1 + 2\cos\frac{2p\pi}{m+1}\right) + \frac{4(\gamma_3+\Delta\gamma_1)}{m+1}\sin^2\frac{p\pi}{m+1}$$

and

$$(\hbar v_{\rm s})^2 = (3d)^2\left[-\frac{1}{2}\gamma_1 s\cos\frac{p\pi}{m+1}\left(\gamma_1 + \gamma_3\left(1+2\cos\frac{2p\pi}{m+1}\right) + \frac{4(\gamma_3+\Delta\gamma_1)}{m+1}\sin^2\frac{p\pi}{m+1}\right) - \gamma_3\left(\gamma_1 + 2\gamma_3\cos\frac{2p\pi}{m+1} + \frac{4(\gamma_3+\Delta\gamma_1)}{m+1}\sin^2\frac{p\pi}{m+1}\right)\right].$$

Here, γ_1=-3.2eV and γ_3=-0.3eV are the nearest neighbor and third nearest neighbor hopping parameters, respectively, $\Delta\gamma_1$=-0.2eV is the correction to γ_1 for the bonds due to edge bond relaxation effect [12], and $\hbar$ is the reduced Planck constant.

The band-structure-limited velocity is proportional to the slope of $E(k)$, $v = (1/\hbar)({\rm d}E/{\rm d}k)$. For each one-dimensional (1D) sub-band of a GNR, the density-of-states (DOS) is inversely proportional to the velocity as $D(E) = 4/hv$. At the ballistic performance limit, the nanotransistor model indicates that the charge density at the top of the potential barrier $\epsilon_{\rm top}$ is

$$N = \int_{-\infty}^{+\infty} \frac{1}{2}\left(\begin{array}{c} D(E-\epsilon_{\rm top}-\Delta/2)f(E-E_{\rm F}) \\ +\, D(E-\epsilon_{\rm top}-\Delta/2)f(E-E_{\rm F}-qV_{\rm D}) \end{array}\right){\rm d}E. \tag{2}$$

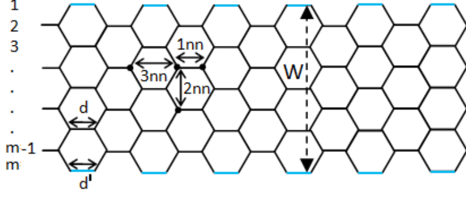

Figure 1: The schematic sketch of an AGNR. The edge of the honeycomb lattice is hydrogen terminated. The edge bonds (colored lines) have a different bonding length and bonding parameter from those in the middle of the AGNR due to edge bond relaxation. The interaction between the first nearest neighbor (1nn), the second nearest neighbor (2nn), and the third nearest neighbor (3nn) atoms are also shown.

The first part is positive velocity states filled by the carriers injected from the source. The second part is negative velocity states filled by the carriers from the drain.

Based on a 2D capacitance model [7], the electrostatics equation is given by

$$\epsilon_{\mathrm{top}} = -q\frac{C_{\mathrm{ins}}V_{\mathrm{G}} + C_{\mathrm{D}}V_{\mathrm{D}} - qN}{C_{\mathrm{ins}} + C_{\mathrm{S}} + C_{\mathrm{D}}}, \tag{3}$$

where C_{ins} is the gate insulator capacitance and C_{S} (C_{D}) is the phenomenological source (drain) capacitance necessary to treat the 2D electrostatic short channel effect.

The current at the ballistic limit is computed as

$$I = \frac{2q\mathrm{k_B}T}{h}\ln\left(\left(1+\mathrm{e}^{\frac{\mathrm{E_F}-\epsilon_{\mathrm{top}}}{\mathrm{k_B}T}}\right)\Big/\left(1+\mathrm{e}^{\frac{\mathrm{E_F}-\epsilon_{\mathrm{top}}-qV_{\mathrm{D}}}{\mathrm{k_B}T}}\right)\right). \tag{4}$$

The edge scattering and optical phonon (OP) scattering [13] have been identified to play an important role in GNRFETs. The carrier scattering is treated in a similar way as described in [7] by computing the transmission coefficient T as

$$T = \begin{cases} \lambda_{\mathrm{edge}}/\left(\lambda_{\mathrm{edge}} + L_{\mathrm{ch}}\right) & \text{if } qV_{\mathrm{D}} < \hbar\omega_{\mathrm{OP}} \\ \frac{\lambda_{\mathrm{edge}}}{\lambda_{\mathrm{edge}} + (\hbar\omega_{\mathrm{OP}}/qV_{\mathrm{D}})L_{\mathrm{ch}}} & \text{if } qV_{\mathrm{D}} > \hbar\omega_{\mathrm{OP}} \end{cases} \tag{5}$$

where L_{ch} is the GNRFET channel length, $\hbar\omega_{\mathrm{OP}} \approx 0.18$eV is the OP energy, and λ_{edge} is the edge scattering mean free path, which is infinitely long for a perfect GNR edge and of the order of GNR width for a rough GNR edge.

3. Results

The electronic properties of the channel material play an important role on GNRFET characteristics. In this section, we first examine the band-gap, band structure, density of states, and band-structure-limited velocity of a GNR. In order to examine the effects of edge bond relaxation and the third nearest neighbor interaction, the simulation results are computed using three models. Model 1 is the simple TB model without edge bond relaxation and the third nearest neighbor interaction, i.e., $\Delta\gamma_1 = \gamma_3 = 0$. Model 2 considers edge bond relaxation only, i.e., $\Delta\gamma_1 = -0.2$eV and $\gamma_3 = 0$. Model 3 considers both effects, i.e., $\Delta\gamma_1 = -0.2$eV and $\gamma_3 = -0.3$eV, and yields the most accurate band structure in agreement with *ab initio* calculations.

Figure 2 plots the band-gap as a function of the GNR width. Without considering edge bond relaxation and the third nearest neighbor interaction, model 1 clearly differentiates GNRs of different widths into two kinds: metallic ($m = 3p+2$) and semiconducting ($m = 3p$ and $m = 3p+1$), which contradicts *ab initio* simulations that indicate narrow AGNRs are all-semiconducting [10–12]. This difference motivates the treatment of edge bond relaxation and the third nearest neighbor interaction in GNRFET modeling. The simulated energy band-gap exhibits three distinct family behaviors. For the AGNR index of $m = 3p+1$, the three models return almost the same result. For $m = 3p$, the results of simple TB and TB with edge bond relaxation are very close, with the third nearest neighbor interaction contributing the largest effect. For these two cases, the band-gap can be expressed analytically by [12]:

$$E_{\mathrm{g}} \approx -2\pi(\gamma_1 - 2\gamma_3)/\sqrt{3}(m+1) \pm 6(\gamma_3 + \Delta\gamma_1)/(m+1), \tag{6}$$

where the plus (minus) sign applies to $m = 3p$ ($m = 3p+1$). When $m = 3p+1$, γ_3 in the first part is almost offset by the second part, and thus the third nearest neighbor interaction contributes a relatively small fraction. As a result, model 3 and model 2 predict similar results. However, when $m = 3p$, γ_3 is the sum of two parts and the effect of the third nearest neighbor interaction is dominant as shown in figure 2. When $m = 3p+2$, the simple TB model fails to yield a band-gap. Both the third nearest neighbor interaction and the edge bond relaxation are responsible for opening a band-gap, with roughly equal contribution from each of them, which can also be observed from an approximate expression [12]:

$$E_{\mathrm{g}} = -6(\gamma_3 + \Delta\gamma_1)/(m+1). \tag{7}$$

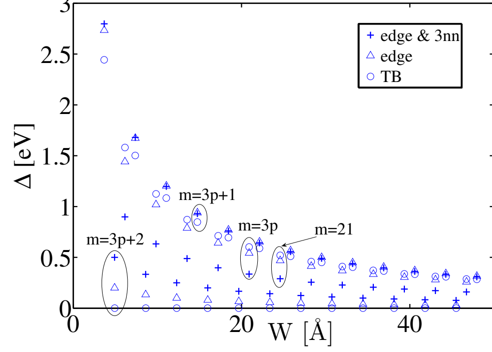

Figure 2: The AGNR band-gap as a function of the GNR width for model 1, the simple tight binding model (circles); model 2, TB with edge bond relaxation only (triangles); and model 3, TB with both edge bond relaxation and third nearest neighbor interaction (crosses). For the group $m = 3p+1$, the three models predict nearly the same results. When $m = 3p$, the third nearest neighbor interaction plays a more important role than edge bond relaxation. When $m = 3p+2$, the third nearest neighbor interaction and edge bond relaxation contribute almost the same effect.

Figure 3 plots the E-k for the 21-AGNR (width = 2.46nm). Comparison between the result computed by model 1 (solid lines) and that computed by model 2 (dashed lines) indicates the small effect of the edge bond relaxation on the band-structure. The third nearest neighbor interaction, however, has a much more pronounced effect on the band-structure, as explained above.

Figure 4 examines the density-of-states for the 21-AGNR (width = 2.46nm). The van Hove singularities appear at the sub-band edges, and the density-of-states is zero in the band-gap energy range. The band-gap computed by model 1 (solid lines) and that computed by model 2 (dashed lines) are close. A decrease of the band-gap is

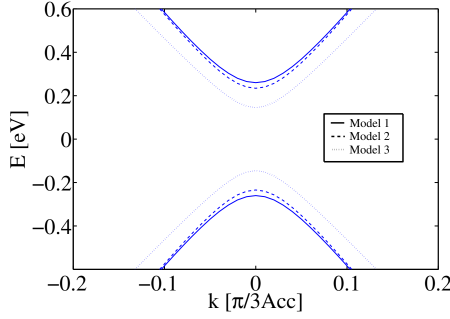

Figure 3: The first sub-band structure of a 21-AGNR (width = 2.46nm) is plotted using three models: model 1 (solid lines), model 2 (dashed lines), and model 3 (dotted lines). Both the third nearest neighbor and edge bond relaxation effects decrease the band-gap. The effect of the third nearest neighbor interaction, however, is larger.

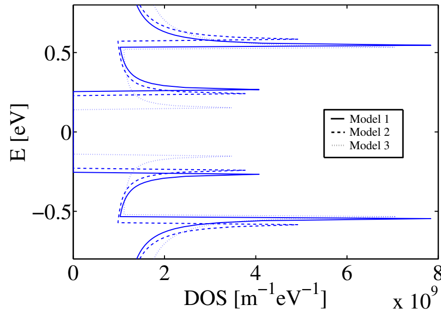

Figure 4: The density-of-states versus the energy for the 21-AGNR (width = 2.46nm) computed using the three models.

clearly observed after the third nearest neighbor interaction is included in model 3. Figure 4 also shows that considering TB with third nearest neighbor and edge bond relaxation will predict higher density-of-states at high energies.

The band-structure-limited velocity versus energy of 21-AGNR as shown in figure 5, which is computed as $v = (1/\hbar)\mathrm{d}E/\mathrm{d}k$. From equation (1), if $E \gg \Delta/2$ the velocity approaches a constant value v_{s}. The results indicate that the third nearest neighbor interaction and the edge bond relaxation effects result in a decrease of the band-structure-limited velocity at high energies. The decrease of the carrier velocity is responsible for an increase of the density-of-states as observed in figure 4.

After studying the effects of the third nearest neighbor interaction and edge bond relaxation on the GNR material properties, we next examine their effect on device characteristics by using the nanotransistor model. The metal-oxide-semiconductor (MOS) gate electrostatics of a GNR is examined first. Figure 6 plots the charge density as a function of the effective gate voltage V_{G} for the 21-AGNR MOS capacitor for three GNR band-structure models. The results indicate the important role of the edge effect and third nearest neighbor on the MOS electrostatics of GNRs. The edge bond relaxation results in a slight decrease of the threshold voltage V_{T}. The third nearest neighbor interaction results in a further and larger decrease of V_{T}, because of the decrease in GNR band-gap. At the same time, the gate capacitance slightly increases after edge effects are considered, due to an increase of the density-of-states as shown in figure 4, which increases the GNR quantum capacitance.

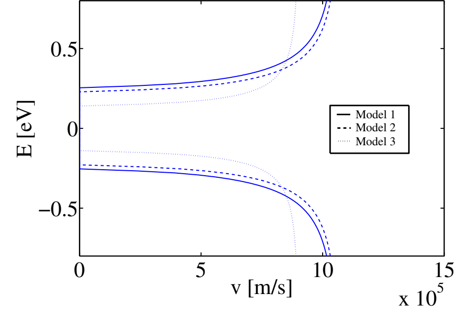

Figure 5: The band-structure-limited carrier velocity for the first sub-band as a function of energy for the 21-AGNR computed using the three models.

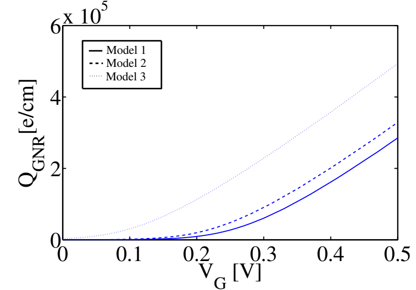

Figure 6: The charge density as a function of the gate voltage at equilibrium ($V_{\mathrm{D}} = 0$) computed using the three models for the 21-AGNR (width = 2.46nm) with $C_{\mathrm{ins}} = 26$pF/m.

Next we analyze the ballistic *I-V* characteristics for GNRFETs with a 21-AGNR channel. As shown in figure 7, including the edge effect and third nearest neighbor effect will both increase the current for the $m = 21$ case. The increase of the current in the 21-AGNRFET is mostly due to the decrease of the band-gap, which manifests itself as the decrease in V_{T} as shown in figure 7(b).

The I-V characteristics in figure 7 are based on an ideal ballistic transport approximation. We next consider the effect of edge scattering. Figure 8 compares the I_{D}-V_{D} characteristics at the ballistic performance limit to the I_{D}-V_{D} characteristics in the presence of edge scattering with a mean free path of 15nm. The current at $V_{\mathrm{D}} = 1$V is about 31% of the ballistic current. On the other hand, our quantum simulations (not shown here) indicate that in the presence of only OP scattering (with an infinitely long edge scattering mean free path achieved for perfect edges), the GNRFET can deliver a near ballistic current, similar to a short-channel CNTFET. It is, therefore, important to improve the edge quality and reduce edge scattering for optimizing the performance of GNRFETs.

4. Summary

A simple analytical model for graphene nanoribbon FETs is developed to examine the effects of edge bond relaxation, the third nearest neighbor interaction, and edge scattering. The results indicate the important role of these edge effects and third nearest neighbor interaction on GNRFET characteristics through band-structure modification and carrier scattering. These effects must be considered in future design and optimization of GNRFETs.

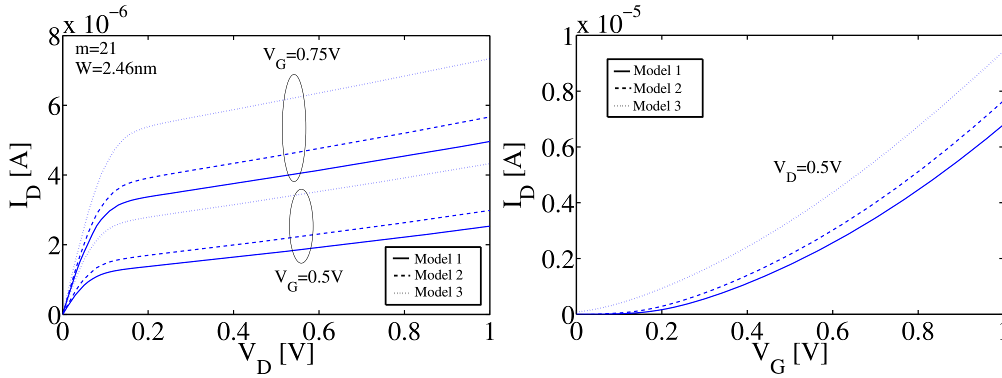

Figure 7: The ballistic (a) $I_{\rm D}-V_{\rm D}$ and (b) $I_{\rm D}-V_{\rm G}$ characteristics computed using the three models for the 21-AGNR with $C_{\rm ins}=26$pF/m and $C_{\rm S}=C_{\rm D}=5$pF/m.

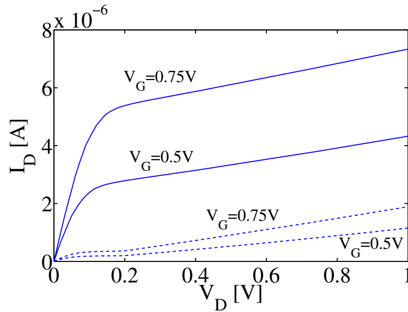

Figure 8: $I-V$ characteristics in the presence of edge scattering is compared with the ideal ballistic approximation for $L_{\rm ch}=100$nm and $\lambda_{\rm edge}=15$nm. The $I_{\rm D}-V_{\rm D}$ curves are for $V_{\rm G}$ = 0.5V and 0.75V.

References

[1] K. S. Novoselov *et al.*, "Electric field effect in atomically thin carbon films," *Science*, vol. 306, pp. 666–669, 2004.

[2] Y. Zhang *et al.*, "Experimental observation of the quantum Hall effect and Berry's phase in graphene," *Nature*, vol. 438, pp. 201–204, 2005.

[3] C. Berger *et al.*, "Electronic confinement and coherence in patterned epitaxial graphene," *Science*, vol. 312, pp. 1191–1196, 2006.

[4] X. Li *et al.*, "Chemically derived, ultrasmooth graphene nanoribbon semiconductors," *Science*, vol. 319, pp. 1229–1232, 2008.

[5] K. Natori, "Ballistic metal-oxide-semiconductor field effect transistor," *Journal of Applied Physics*, vol. 76, no. 8, pp. 4879–4890, 1994.

[6] A. Raychowdhury, S. Mukhopadhyay, and K. Roy, "A circuit-compatible model of ballistic carbon nanotube field-effect transistors," *IEEE Trans. Computer-aided Design*, vol. 23, pp. 1411–1420, Oct. 2004.

[7] M. Lundstrom and J. Guo, *Nanoscale Transistors: Device Physics, Modeling and Simulation*. New York, NY: Springer, 2006.

[8] H.-S. P. Wong *et al.*, "Carbon nanotube transistor circuits: Models and tools for design and performance optimization," in *Proc. Intl. Conference Computer-aided Design*, pp. 651–654, 2006.

[9] H. Hashempour and F. Lombardi, "Device model for ballistic CNFETs using the first conducting band," *IEEE Design and Test of Computers*, vol. 25, pp. 178–186, 2008.

[10] Y.-W. Son, M. L. Cohen, and S. G. Louie, "Energy gaps in graphene nanoribbons," *Physical Review Letters*, vol. 97, p. 216803, 2006.

[11] C. T. White *et al.*, "Hidden one-electron interactions in carbon nanotubes revealed in graphene nanostrips," *Nano Letters*, vol. 7, pp. 825–830, 2007.

[12] D. Gunlycke and C. T. White, "Tight-binding energy dispersions of armchair-edge graphene nanostrips," *Physical Review B*, vol. 77, p. 115116, 2008.

[13] X. Wang *et al.*, "Room temperature all-semiconducting sub-10nm graphene nanoribbon field-effect transistors," *Physical Review Letters*, vol. 100, p. 206803, 2008.